

Enhanced Sensitivity Carbon Nanotubes as Targeted Photoacoustic Molecular Imaging Agents

Adam de la Zerda^{1,2,*}, Zhuang Liu^{3,*}, Cristina Zavaleta¹, Sunil Bodapati¹, Robert Teed¹,
Srikant Vaithilingam², Te-Jen Ma², Omer Oralkan², Xiaoyuan Chen¹, Butrus T. Khuri-Yakub²,
Hongjie Dai^{3,†}, Sanjiv S. Gambhir^{1,4,†}

¹Molecular Imaging Program at Stanford, Department of Radiology and Bio-X Program, the

²Department of Electrical Engineering, the ³Department of Chemistry and the ⁴Department of
Bioengineering, Stanford University, Palo Alto, CA 94305, USA.

ABSTRACT

Photoacoustic imaging of living subjects offers high spatial resolution at increased tissue depths compared to purely optical imaging techniques. We have recently shown that intravenously injected single walled carbon nanotubes (SWNTs) can be used as targeted photoacoustic imaging agents in living mice using RGD peptides to target $\alpha_v\beta_3$ integrins. We have now developed a new targeted photoacoustic imaging agent based on SWNTs and Indocyanine Green (SWNT-ICG) with absorption peak at 780nm. The photoacoustic signal of the new imaging agent is enhanced by ~20 times as compared to plain SWNTs. The particles are synthesized from SWNT-RGD that non-covalently attach to multiple ICG molecules through pi-pi stacking interactions. Negative control particles had RAD peptide instead of RGD. We measured the serum stability of the particles and verified that the RGD/RAD conjugation did not alter the particle's absorbance spectrum. Finally, through cell uptake studies with U87MG cells we verified that the particles bind selectively to $\alpha_v\beta_3$ integrin. In conclusion, the extremely high absorption of the SWNT-ICG particles shows great promise for high sensitivity photoacoustic imaging of molecular targets in-vivo. This work lays the foundations for future in-vivo studies that will use the SWNT-ICG particles as imaging agents administered systemically.

Contact information: sgambhir@stanford.edu

* These authors contributed equally to this work

† e-mail: sgambhir@stanford.edu; hdai@stanford.edu

INTRODUCTION

Photoacoustic imaging is an emerging imaging modality that overcomes, to a great extent, the resolution and depth limitations of optical imaging but maintains the high-contrast of optics¹. When a short light pulse is used to illuminate tissues, the light is scattered and absorbed as it propagates through the tissues. The absorbed light is converted into heat, which in return causes the material to locally expand, creating a pressure wave. The pressure wave can then be detected by an ultrasound system placed outside the subject of interest. By measuring the pressure waves from several positions, a full tomographic image can be reconstructed. This way, light only has to propagate into the tissue, and sound, which is minimally absorbed and scattered by tissues in low frequencies, propagates out of the tissue. Therefore, the depth of imaging can reach up to ~5 cm, a marked increase compared to optical imaging techniques². Photoacoustic imaging of living subjects has been used to image endogenous signals such as melanomas³, thermal burns⁴, and oxygenation levels of blood⁵. However, most diseases will not manifest an endogenous photoacoustic contrast. Therefore, in order to fully utilize the potential of photoacoustic imaging, it is essential to inject an exogenous photoacoustic contrast agent (molecular imaging agent) that targets the diseased area(s) in the subject of interest. The ideal molecular imaging agent will have a sufficiently large optical absorption cross section to maximize the agent's photoacoustic signal, but yet be small enough to escape uptake by the reticuloendothelial system (RES), specifically the liver and the spleen. However, designing such an imaging agent is not trivial since a particle's absorption cross section and its size are highly correlated.

Recently, we showed that single walled carbon nanotubes (SWNTs) have utility as photoacoustic contrast agents⁶. SWNTs have strong light absorption characteristics and may act as photoacoustic contrast agents. SWNTs can be made as small as 1 nm in diameter but yet their length can extend to hundreds of nanometers increasing their absorption cross section and their intrinsic photoacoustic contrast. This unique geometry of SWNTs led to several applications of SWNTS in nanomedicine including drug delivery⁷ and photothermal therapy⁸. Here we present a new photoacoustic contrast agent based on SWNTs that have indocyanine green (ICG) molecules bound to their surface (SWNT-ICG). This increases the photoacoustic contrast by up to 20 times compared to plain

SWNTs due to much stronger light absorption characteristics. Furthermore, the absorption peak of the SWNT-ICG particles is conveniently located at 780nm, a wavelength at which tissue optical absorption and therefore photoacoustic background signal are minimal.

1. METHODS AND MATERIALS

SWNT-ICG-RGD conjugates synthesis. A complete description of the synthesis of SWNT-RGD and SWNT-RAD can be found elsewhere⁹. SWNT-RGD and SWNT-RAD were then incubated with excess of ICG molecules dissolved in DMSO overnight. Unbound ICG molecules were removed from the solution by filtration of the SWNT particles. The SWNTs used in this work were 50-300 nm in length and 1-2 nm in diameter. The molar concentrations¹⁰ are based on an average molecular weight of 170 kDa per SWNT (150 nm in length and 1.2 nm in diameter).

Photoacoustic imaging instrument. Our photoacoustic system¹¹ is illustrated in **Fig. 1**. A tunable pulsed laser with a repetition rate of 10 Hz and a pulse width of 5 ns (Nd:YAG Surelight-III-10 connected to Surelite OPO Plus, Continuum) illuminated the object through a fiber optic ring light (50-1353 Ringlight, Fiberoptic Systems Inc.). The average energy density of the laser at 690 nm wavelength was measured to be ~ 9 mJ/cm² at the target site, which is below the ANSI limitation for laser skin exposure¹². A 5 MHz focused transducer (25.5 mm focal length, 4 MHz bandwidth, F number of 2.0, depth of focus of 6.5 mm, lateral resolution of 600 μ m, and axial resolution of 380 μ m. A309S-SU-F-24.5-MM-PTF, Panametrics) was used to acquire both pulse-echo and photoacoustic images. In addition, high resolution ultrasound images were acquired using a 25 MHz focused transducer (27 mm focal length, 12 MHz bandwidth, F number of 4.2, depth of focus of 7.5 mm, lateral resolution of 250 μ m, and axial resolution of 124 μ m. V324-SU-25.5-MM, Panametrics). A precision xyz-stage (U500, Aerotech Inc.) with minimum step size of 1 μ m was used to move the transducer and the fiber ring along a planar 2D trajectory. At every position, the acquired signal was averaged over 16 laser pulses. The time of arrival and the intensity of the laser pulses were recorded using a silicon photodiode (DET10A, Thorlabs). This information was used to synchronize the acquisition and compensate for pulse-to-pulse variations in laser intensity. The analog photoacoustic signals were amplified using a tunable preamplifier (Panametrics) and digitized using an

oscilloscope (Infiniium 54825A, Agilent). The photoacoustic and ultrasound images were reconstructed as follows: the a-scan from each position of the transducer was band pass filtered with 100% fractional bandwidth, compensated for laser intensity variation and envelope detected. The a-scans were then combined to reconstruct a 3D intensity image of the target. No further post-processing was done on the images. The ultrasound images acquired using the 5 MHz and 25 MHz transducers were aligned together using small vertical translations so that the object's skin level matches in both images. Then, photoacoustic and the high frequency ultrasound images were analyzed, co-registered and displayed using AMIDE¹³ software.

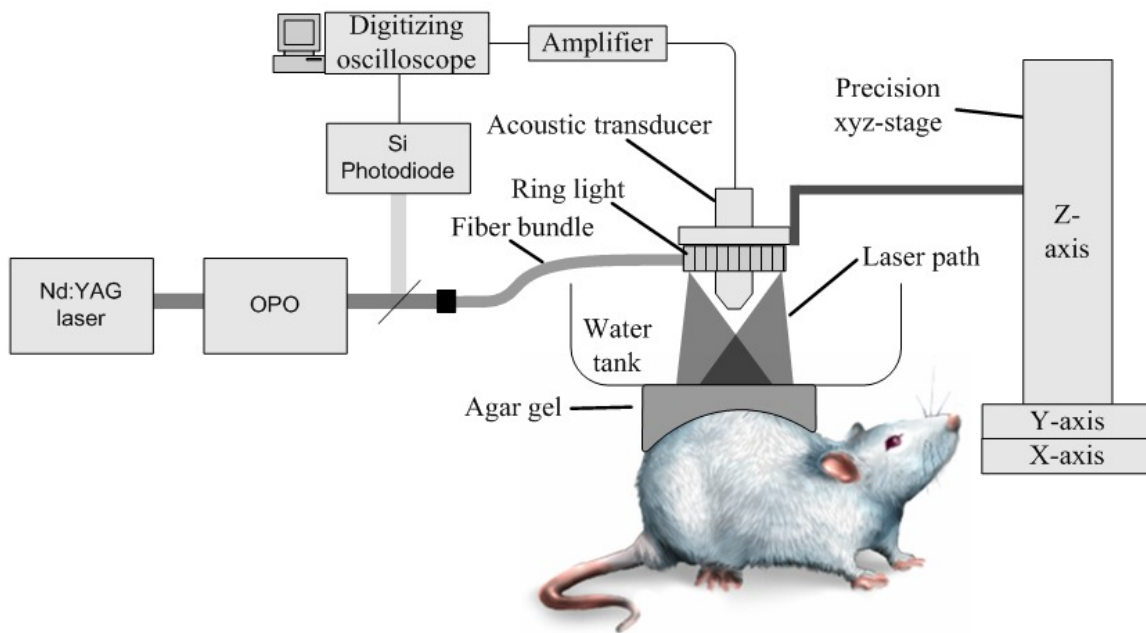


Figure 1 Photoacoustic imaging instrument. A tunable pulsed laser (Nd:YAG laser and OPO) illuminated the subject through a fiber optic ring light. The photoacoustic signals produced by the sample were acquired using a 5 MHz focused transducer. A precision xyz-stage was used to move the transducer and the fiber ring along a planar 2D trajectory. The time of arrival and the intensity of the laser pulses were recorded using a silicon photodiode. This information was used to synchronize the acquisition and compensate for pulse-to-pulse variations in laser intensity. The analog photoacoustic signals were amplified using a 40 dB preamplifier and digitized using an oscilloscope.

2. RESULTS

Optical characterization of SWNT-ICG. We have measured the optical absorption spectrum of the SWNT-ICG particles (**Fig. 2**). Importantly, the absorption spectra of both SWNT-ICG-RGD and SWNT-ICG-RAD were found to be nearly identical, suggesting that the RGD/RAD peptide does not affect. The absorption spectra of the particles peak at 780nm, and represent a 20-fold improvement in absorption over plain SWNTs.

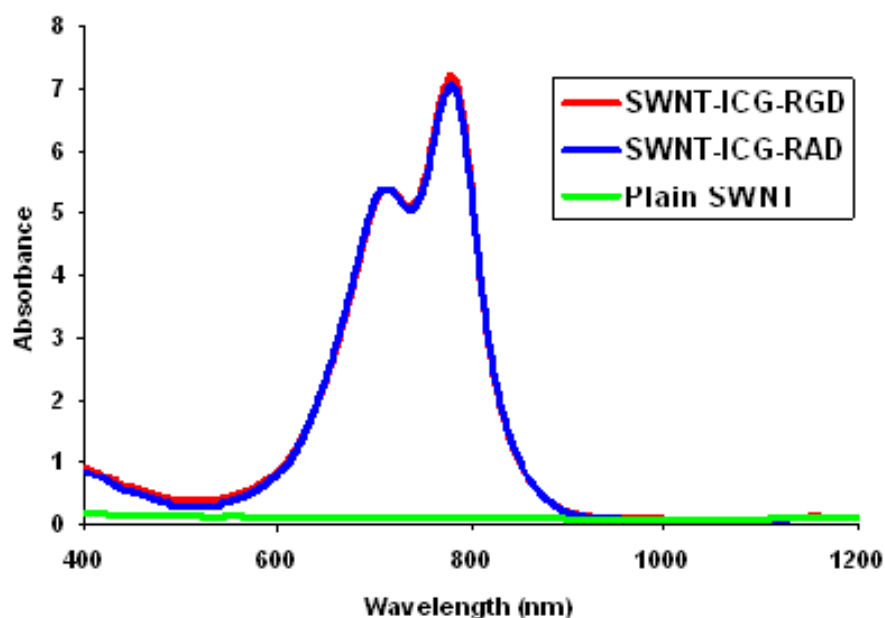


Figure 2 - Characterization of SWNT photoacoustic properties. a, The optical absorption spectra of plain SWNT (green), SWNT-ICG-RGD (red) and SWNT-ICG-RAD (blue). The spectral overlap between SWNT-ICG-RGD and SWNT-ICG-RAD suggests that the peptide conjugation does not perturb their spectra.

SWNT-ICG Serum Stability. We incubated 2.5nM of SWNT-ICG-RAD with 10% serum and 90% PBS and monitored the optical absorbance of the solution at wavelength of 780nm every 3 minutes for duration of 2.5 hrs. Control solutions included 10% serum only or 2.5nM of SWNT-ICG-RAD

only. Throughout the 2.5 hours, the absorbance of all solutions remained the same and did not deviated more than 5% ($p < 0.05$).

Cell uptake study. We exposed 1×10^6 $\alpha_v\beta_3$ expressing cells (U87MG) to SWNT-ICG-RGD and SWNT-ICG-RAD for increased durations of time from 10 min up to 4 hours. Control cells were exposed to SWNT-ICG-RAD. After exposure, the cells were washed with saline to remove unbound particles and scanned using a highly sensitive spectrophotometer for their absorbance at 780nm. After 2 hours of incubation, U87MG cells exposed to SWNT-ICG-RGD were found to have 95% higher absorbance than cells exposed to SWNT-ICG-RAD ($p < 0.05$) indicating the specific binding of the RGD-targeted particles to the $\alpha_v\beta_3$ receptor in contrast with the control particles. Furthermore, after 2 hours of incubation, the number of particles bound to the cell reached a maximum, and hence 2 hours of incubation was concluded to be the optimal time point.

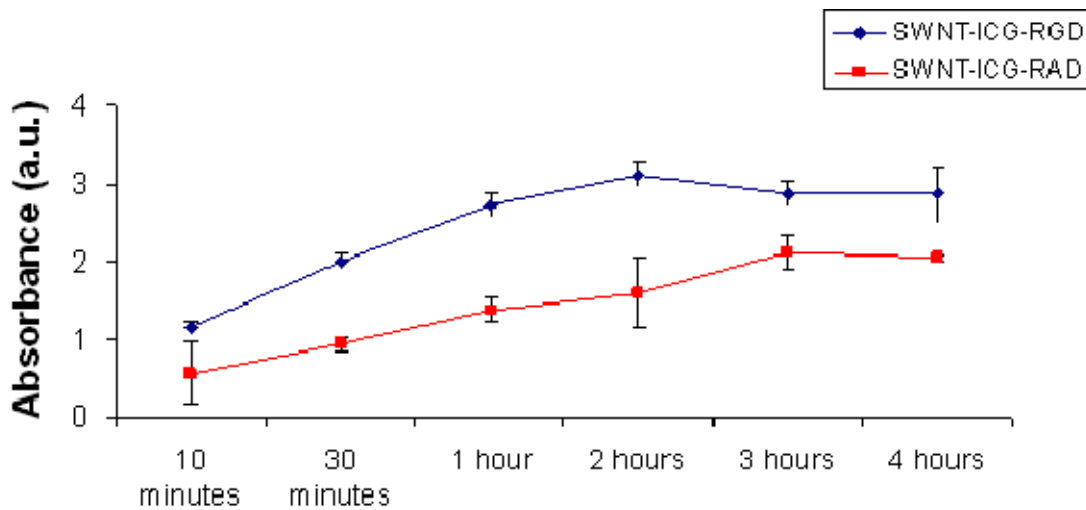


Figure 3 – SWNT-ICG cell uptake studies. U87MG incubated with SWNT-ICG-RGD showed over 95% higher signal than U87 cell incubated with SWNT-ICG-RAD in the first 4 time points, and then dropped to 35% for 3 and 4 hours incubation times ($p < 0.05$ for each time point independently).

3. DISCUSSION AND CONCLUSION

The absorption spectra of the SWNT-ICG particles peak at 780nm, and represent a 20-fold improvement in absorption over plain SWNTs. Importantly, since blood optical absorption is minimized at ~780nm then so is the photoacoustic background signal leading to even higher sensitivity. Finally, these new imaging agents bring promise to significantly increase the sensitivity of photoacoustic imaging agents for in-vivo use.

ACKNOWLEDGEMENTS

This work was supported, in part, by NCI CCNE U54 (SSG) and NCI ICMIC P50 CA114747 (SSG).

REFERENCES

1. Xu, M.H. & Wang, L.H.V. Photoacoustic imaging in biomedicine. *Rev. Sci. Instrum.* **77**, 041101-043100 (2006).
2. Ku, G. & Wang, L.V. Deeply penetrating photoacoustic tomography in biological tissues enhanced with an optical contrast agent. *Opt. Lett.* **30**, 507-9 (2005).
3. Oh, J.T. et al. Three-dimensional imaging of skin melanoma in vivo by dual-wavelength photoacoustic microscopy. *J. Biomed. Opt.* **11**, 34032 (2006).
4. Zhang, H.F., Maslov, K., Stoica, G. & Wang, L.V. Imaging acute thermal burns by photoacoustic microscopy. *J. Biomed. Opt.* **11**, 054033 (2006).
5. Wang, X., Xie, X., Ku, G., Wang, L.V. & Stoica, G. Noninvasive imaging of hemoglobin concentration and oxygenation in the rat brain using high-resolution photoacoustic tomography. *J. Biomed. Opt.* **11**, 024015 (2006).
6. De la Zerda, A. et al. Carbon nanotubes as photoacoustic molecular imaging agents in living mice. *Nat Nanotechnol* **3**, 557-62 (2008).
7. Liu, Z., Sun, X., Nakayama-Ratchford, N. & Dai, H. Supramolecular Chemistry on Water-Soluble Carbon Nanotubes for Drug Loading and Delivery. *ACS Nano.* **1**, 50-56 (2007).
8. Son, S.J., Bai, X. & Lee, S.B. Inorganic hollow nanoparticles and nanotubes in nanomedicine Part 2: Imaging, diagnostic, and therapeutic applications. *Drug Discov. Today* **12**, 657-63 (2007).

9. Liu, Z. et al. In vivo biodistribution and highly efficient tumour targeting of carbon nanotubes in mice. *Nat. Nano.* **2**, 47-52 (2007).
10. Kam, N.W., O'Connell, M., Wisdom, J.A. & Dai, H. Carbon nanotubes as multifunctional biological transporters and near-infrared agents for selective cancer cell destruction. *Proc. Natl. Acad. Sci. U. S. A.* **102**, 11600-5 (2005).
11. Vaithilingam, S. et al. in Ultrasonics Symposium, 2007. IEEE 2413-2416 (2007).
12. American National Standards Institute, American national standard for the safe use of lasers, *ANSI Standard Z136.1-2000*, ANSI, Inc., New York. (2000).
13. Loening, A.M. & Gambhir, S.S. AMIDE: a free software tool for multimodality medical image analysis. *Mol. Imaging* **2**, 131-7 (2003).